NUREG/CR-6071
ORNL/TM-12406

Impact of ENDF/B-VI Cross-Section Data on H. B. Robinson Cycle 9 Dosimetry Calculations

Prepared by
M. L. Williams, M. Asgari, F. B. K. Kam

Oak Ridge National Laboratory

Prepared for
U.S. Nuclear Regulatory Commission

AVAILABILITY NOTICE

Availability of Reference Materials Cited in NRC Publications

Most documents cited in NRC publications will be available from one of the following sources:

1. The NRC Public Document Room, 2120 L Street, NW, Lower Level, Washington, DC 20555-0001

2. The Superintendent of Documents, U.S. Government Printing Office, Mail Stop SSOP, Washington, DC 20402-9328

3. The National Technical Information Service, Springfield, VA 22161

Although the listing that follows represents the majority of documents cited in NRC publications, it is not intended to be exhaustive.

Referenced documents available for inspection and copying for a fee from the NRC Public Document Room include NRC correspondence and internal NRC memoranda; NRC Office of Inspection and Enforcement bulletins, circulars, information notices, inspection and investigation notices; Licensee Event Reports; vendor reports and correspondence; Commission papers; and applicant and licensee documents and correspondence.

The following documents in the NUREG series are available for purchase from the GPO Sales Program: formal NRC staff and contractor reports, NRC-sponsored conference proceedings, and NRC booklets and brochures. Also available are Regulatory Guides, NRC regulations in the *Code of Federal Regulations*, and *Nuclear Regulatory Commission Issuances*.

Documents available from the National Technical Information Service include NUREG series reports and technical reports prepared by other federal agencies and reports prepared by the Atomic Energy Commission, forerunner agency to the Nuclear Regulatory Commission.

Documents available from public and special technical libraries include all open literature items, such as books, journal and periodical articles, and transactions. *Federal Register* notices, federal and state legislation, and congressional reports can usually be obtained from these libraries.

Documents such as theses, dissertations, foreign reports and translations, and non-NRC conference proceedings are available for purchase from the organization sponsoring the publication cited.

Single copies of NRC draft reports are available free, to the extent of supply, upon written request to the Office of Information Resources Management, Distribution Section, U.S. Nuclear Regulatory Commission, Washington, DC 20555-0001.

Copies of industry codes and standards used in a substantive manner in the NRC regulatory process are maintained at the NRC Library, 7920 Norfolk Avenue, Bethesda, Maryland, and are available there for reference use by the public. Codes and standards are usually copyrighted and may be purchased from the originating organization or, if they are American National Standards, from the American National Standards Institute, 1430 Broadway, New York, NY 10018.

NUREG/CR-6071
ORNL/TM-12406
R5

Impact of ENDF/B-VI Cross-Section Data on H. B. Robinson Cycle 9 Dosimetry Calculations

Manuscript Completed: September 1993
Date Published: October 1993

Prepared by
M. L. Williams*, M. Asgari*, F. B. K. Kam

Oak Ridge National Laboratory
Operated by Martin Marietta Energy Systems, Inc.

Oak Ridge National Laboratory
Oak Ridge, TN 37831-6285

Prepared for
Division of Engineering
Office of Nuclear Regulatory Research
U.S. Nuclear Regulatory Commission
Washington, DC 20555-0001
NRC FIN B0415

*Louisiana State University Nuclear Science Center
Baton Rouge, LA 70803

ABSTRACT

Dosimeters that were removed from the H. B. Robinson reactor following Cycle 9 were analyzed and compared with calculated results in an earlier study. This work updates the calculation using recently available ENDF/B-VI data in order to assess advantages to using the newer cross sections in reactor pressure vessel fluence calculations. A comparison is also made to determine the impact of various cross-section libraries on computed dosimeter activities.

Significant improvements are obtained with the ENDF/B-VI cross sections. Other factors, such as differences in group structures of multigroup libraries, may also affect the calculated dosimeter activities.

CONTENTS

LIST OF FIGURES

LIST OF TABLES

ACKNOWLEDGMENTS

The authors acknowledge the technical and financial support of C. Z. Serpan and Al Taboada of the Nuclear Regulatory Commission; E. Sajo and I. Remec for their suggestions in reviewing this report; L. P. Hileman for preparing the manuscript; and C. H. Shappert for editing.

1 INTRODUCTION

Two earlier studies performed by the Oak Ridge National Laboratory (ORNL) for the U.S. Nuclear Regulatory Commission (NRC) have provided estimates for the neutron exposure to the reactor pressure vessel (RPV) of the H.B. Robinson (HBR) PWR. The first of these two studies compared results of transport calculations with measured activities of surveillance dosimeters located at both in vessel and reactor cavity positions during Cycle 9.[1] The second ORNL study consisted of transport calculations to determine the fluence rate for HBR Cycle 10, which was the first cycle to utilize "partial length shield assemblies" (PLSAs) as a means of RPV flux reduction. In the latter study, the transport calculations were compared with experimental measurements of various dosimeters located only within the reactor cavity.[2] In both of these earlier studies, inconsistencies were observed between the calculated and measured dosimeter activities in the cavity region.

The Cycle 9 transport calculations were performed by Maerker and used the ELXSIR[3] multigroup cross-section library, which is based on ENDF/B-IV data. A detailed sensitivity-uncertainty analysis using the LEPRICON[1] system was performed as part of the study, and these calculations suggested that most of the observed discrepancies were due to the iron inelastic cross section in ENDF/B-IV, which causes high-energy threshold reactions to be underestimated in the cavity.

The Cycle 10 analysis was performed during 1989, approximately four years after the original Cycle 9 study. The Cycle 10 study used a modified version of the SAILOR cross-section library,[4] which contained newer iron data based on a revised evaluation provided by C. Y. Fu of ORNL.[5] This evaluation has been designated unofficially as the "REV-V" iron data.[6] It was found that the REV-V iron cross sections used for the Cycle 10 transport calculations significantly increased the transmission of the fast flux through the HBR vessel compared with the ENDF/B-IV or ENDF/B-V iron evaluations, such as those evaluations used in the earlier Cycle 9 calculations. This REV-V iron cross section increases the calculated values for the higher threshold reactions, such as ^{54}Fe(n,p) and ^{58}Ni(n,p), and improves the agreement with the cavity measurements of these dosimeters. However, some inconsistencies still were unresolved, especially for the lower threshold ^{237}Np(n,f) dosimeter. It appears that the Fu REV-V iron evaluation does not significantly increase the calculated value for this dosimeter reaction, which unlike the iron and nickel dosimeters, is sensitive to the energy range between 0.5 and 2.0 MeV. Thus the computed neptunium activity remains substantially low relative to the experimental measurement while the iron and nickel value are computed much closer to the respective experimental results. This relationship suggests that the REV-V iron data may introduce a bias between the high-threshold and low-threshold reactions calculated in the cavity (which was not observed with the ENDF/B-IV or ENDF/B-V iron data). Because of increasing importance of cavity dosimetry in assessing pressure vessel fluence, it is very important to establish a reliable set of iron data that can be used as a standard for transport calculations. Neither the ENDF/B-IV or ENDF/B-V, which are the bases of the widely used SAILOR and ELXSIR multigroup libraries, nor the REV-V data utilized in the HBR Cycle 10 analysis, appears to be completely satisfactory in this regard.

In 1989, the most recent version of the ENDF/B was released by the National Nuclear Data Center (NNDC): ENDF/B-VI. This data file includes new iron cross-section evaluations that evolved from the earlier REV-V evaluation developed by Fu. Compared with earlier ENDF/B versions, the version VI iron evaluation gives a forward bias to the inelastic scatter kernel, and the magnitude of the inelastic cross section is reduced somewhat. Also, nuclear data are given for each of the iron isotopes, rather than for the composite "natural iron." These values allow for a more accurate treatment of the self-shielding. These changes in the iron data will significantly impact the neutron transmission through the RPV. Preliminary results obtained in an earlier study suggest that ENDF/B-VI iron data will increase the computed dosimeter activities in the cavity of power reactors without introducing a bias between the high and lower threshold reaction rates, such as observed with the REV-V evaluation.[6] However, this conclusion is based only on projections obtained from one-dimensional (1-D) calculations. No complete two-dimensional (2-D) calculation of a power reactor has been performed with ENDF/B-VI.

The objective of this study is to perform an updated calculation for H. B. Robinson Cycle 9 using selected ENDF/B-VI cross-section data. Specifically, the iron isotopes ^{54}Fe, ^{56}Fe, ^{57}Fe, and ^{58}Fe, and oxygen and hydrogen — are all represented by ENDF/B-VI data. Data for all other materials are taken from the original SAILOR library, which is based on ENDF/B-IV. The results of this analysis will be important in assessing the merit of utilizing ENDF/B-VI for RPV fluence determination, and will help in deciding whether a new cross-section library based on

ENDF/B-VI should replace the older libraries based on versions IV and V that are widely used in industry today. These results are given in Section 3. This report also sumarizes results of a study aimed at understanding the differences observed in calculations performed with two commonly used cross-section libraries. The SAILOR and ELXSIR data libraries are used in many RPV fluence analysis studies, so it is important to understand any discrepancies that may be attributed to the libraries themselves. The impact of differences in self-shielding assumptions and collapsing spectra curve are considered, in addition to the inherent variations due to different group structures. Spectral differences for both high threshold dosimeters like $^{54}Fe(n,p)$ and $^{58}Ni(n,p)$ and lower threshold dosimeters like $^{237}Np(n,f)$ and $^{238}U(n,f)$ in a one-dimensional model of H. B. Robinson are considered. These results are summarized in Section 4.

2 CALCULATION METHODOLOGY

The same method as used in the previous HBR transport calculations (and in many other studies) was also used in the current work. Basically, this consists of synthesizing a three-dimensional (3-D) flux distribution from results obtained in 1- and 2-D DOT discrete-ordinates calculations. Details of these synthesis calculations are given in the references.[1,2] The core source was based on the mid-cycle (MOC) distribution for Cycle 9. The spatial variation of the source is obtained by combining a pinwise relative power distribution with the absolute assembly-wise powers to determine the absolute pin-wise power at MOC. This distribution is mapped onto a $R\theta$ coordinate system used in the transport calculations. The conversion factor from power density to neutron source density is based on the average burnup of the peripheral assemblies in order to reflect the proper contributions of ^{239}Pu and ^{235}U to the fission source. Similarly, the fission spectrum is a weighted combination of these two isotopes at the appropriate burnup condition. Extension of the mid-cycle calculations to end of cycle (EOC) was done by multiplying by EOC-to-MOC ratios reported by Maerker[1] in his earlier Cycle 9 analysis.

The transport model used in this analysis is virtually identical to that used in Maerker's earlier Cycle 9 analysis, except near the 45° azimuth, where an additional "detector well" is included within the cavity region. Figure 2.1 shows the $R\Theta$ model of the one-eighth HBR core. Note the presence of the two large cavity "wells" within the concrete center wall of the cavity at 0° and 45°. The wells affect the flux spectrum near these locations and cause difficulty in utilizing 1-D or RZ calculations to estimate the flux spectrum in the cavity, because the wells cannot be represented with axisymmetric geometries.

The cross-section library used in the calculations was a modified version of the 47-neutron group SAILOR library. The original SAILOR library was collapsed from the ENDF/B-IV VITAMIN-C library,[7] the same fine-group library that was collapsed to create the 56-group ELXSIR library used in Maerker's earlier analysis of the HBR Cycle 9 dosimetry. The modified SAILOR library contains additional cross sections for iron, oxygen, and hydrogen (Fe-O-H) that were processed from ENDF/B-VI data by J. E. White of ORNL, using the same processing methodology as for the original SAILOR. Calculations were performed with both the original SAILOR and the ENDF/B-VI Fe-O-H cross sections, for comparison with the earlier results obtained with ELXSIR.

Figure 2.2 shows the ratios of the iron inelastic cross section in REV-V and ENDF/B-VI, respectively, to the ENDF/B-V values (which are essentially the same as version IV in the energy range of interest here). The ENDF/B-VI data are about 10% lower than ENDF/B-V cross sections between 0.5 and 0.86 MeV, and are up to 14% lower in the energy range between 2.5 and 6.0 MeV. The REV-V inelastic data are also much lower than ENDF/B-V between 3.5 and 6.0 MeV (even more so than version VI); however, there is no difference between the REV-V and ENDF/B-V below 2.5 MeV. The cross sections in the higher energy interval affect the neutron spectrum in the range to which the $^{54}Fe(n,p)$ and $^{58}Ni(n,p)$ threshold reactions are most sensitive, whereas the $^{237}Np(n,f)$ is sensitive to the energy range from 0.5 to 2.0 MeV. The differences in the REV-V and ENDF/B-VI inelastic cross section in this lower energy interval will cause the two data files to affect the calculated Np reaction rate differently.

Because of the close similarity between the present transport calculations and those in the early Cycle 9 analysis, the difference observed in the results from the two studies will reflect primarily the impact of version VI versus IV nuclear data. However, variations in the multigroup processing procedures and group structures of the SAILOR and ELXSIR cross-section libraries will also cause some discrepancies. A separate study using 1-D calculations

was performed to investigate the effect of various resonance self-shielding, cross-section weighting spectra, and group-structure differences on the computed results. The one-dimensional model used in the transport calculations was the same as used in the synthesis calculation.

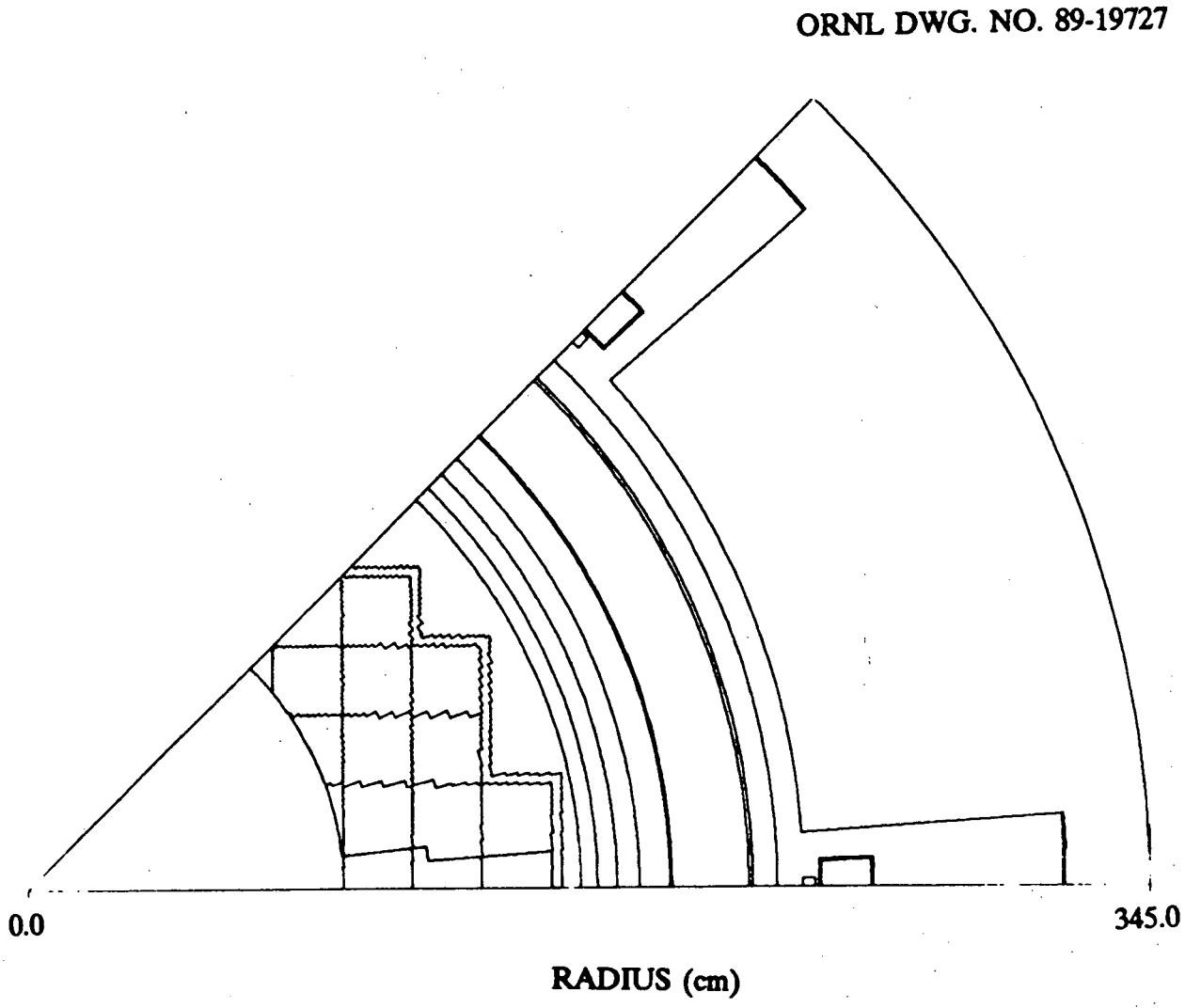

Figure 2.1 DOT RΘ model of H. B. Robinson Unit 2.

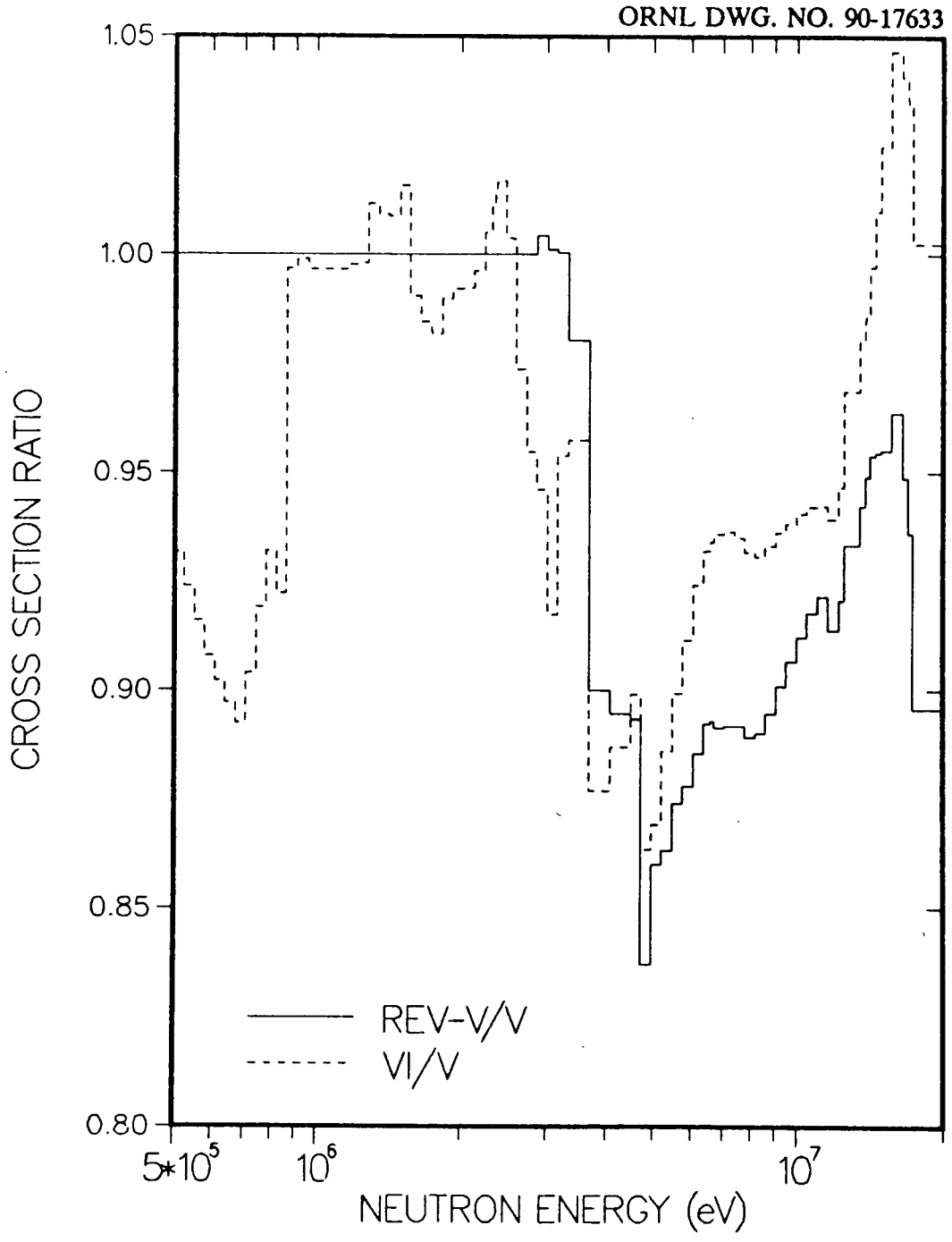

Figure 2.2 Ratio of REV-V and ENDF/B-VI inelastic multigroup cross sections to the ENDF/B-V values (natural iron).

3 RESULTS FOR HBR CYCLE 9

Tables 3.1 and 3.2, respectively, show the absolute flux spectra at the surveillance location (20°) in the downcomer and at the cavity location (0°) obtained with the modified SAILOR library which contains ENDF/B-VI Fe-O-H data. The absolute dosimeter reaction rates computed with these spectra are given in Table 3.3. The values in Table 3.3 were obtained with the ENDF/B-VI file. In calculating the dosimeter activities, two different sets of dosimetry cross sections were used. One is based on the cross sections taken from ENDF/B-VI. The other, designated as the "original dosimetry file," corresponds to data taken from the LSLM-2 adjustment code, file C91. The major difference is in the $^{63}Cu(n,a)$ reaction, which is known to be too large in the earlier dosimetry file.

Table 3.4 compares our results computed using the *original* SAILOR library with Maerker's earlier values calculated with ELXSIR cross sections. Recall that both of these libraries are based on the same ENDF/B-IV data and should be expected to give similar results. In the downcomer region, the original SAILOR and the ELXSIR results agree well using either set of dosimetry data, except for the $^{63}Cu(n,\alpha)$ value which is overpredicted by about 22% with the original dosimeter cross section data. This discrepancy in the earlier ^{63}Cu dosimetry data is well known and explains this difference. However, something strange happens in the cavity region: the original SAILOR calculations with both dosimetry files give about a 20 to 25% lower value than Maerker's ELXSIR results for the ^{237}Np reaction. All other threshold reactions computed with the original SAILOR and the ELXSIR libraries agree well. This variation suggests that the neutron spectra calculated with the two respective libraries for the cavity are significantly different in the energy range below 2.0 MeV, even though both libraries are based on ENDF/B-IV. As discussed in the next section, there appears to be about a 20% discrepancy in the flux above 0.1 MeV calculated with ELXSIR and the original SAILOR, respectively, that is presumably caused by the coarser group structure in SAILOR. ELXSIR agrees better with fine-group results, which are assumed to be the most accurate calculations.

Tables 3.5 and 3.6 show that the ENDF/B-VI Fe-O-H increase the original SAILOR values of the calculated dosimeter activities in the cavity by about 30 to 35%, except for the very high-threshold $^{63}Cu(n,\alpha)$, which only increases about 20%. This dosimeter behaves differently than the others because of its higher sensitivity in the energy range above 10.0 MeV, where the ENDF/B-VI iron inelastic cross section does not decrease as much compared with the earlier ENDF versions. The cross section around 14.0 MeV is actually higher in version VI than version V (see Fig. 2.2). These changes for the various dosimeters are more uniform and consistent than found earlier for the Cycle 10 analysis where the REV-V iron data were used. For example, it was found that the REV-V data increased the ^{54}Fe dosimeter activity by 60% and the ^{237}Np activity by only 28%, whereas the ENDF/B-VI data increased the two dosimeter activities by 35% and 32%, respectively.

Finally, the revised C/E values obtained for HBR Cycle 9 are shown in Table 3.7. Experimental values were obtained from reference 9. Computed activities in the cavity region are significantly underestimated with both the ELXSIR and original SAILOR libraries. However, it can be seen that the ENDF/B-VI results show excellent agreement with measured dosimeter results at both the downcomer and cavity locations. Most C/E's are within 5% of unity. A notable exception is the cavity ^{237}Np value, which is still not consistent with the other values. Based on the analysis described in the next section, it is felt that the SAILOR calculation of the ^{237}Np dosimeter is probably about 10 to 15% too low due to group structures and/or multigroup processing approximations. Even after applying this correction, the neptunium C/E value will remain about 30% lower than the other dosimeter results. We feel that this residual discrepancy is probably caused by a measurement problem in the HBR Cycle 9 experiment for the neptunium dosimeter.

The new HBR results are consistent with earlier studies that projected that ENDF/B-VI iron cross sections would significantly improve the calculations of cavity dosimetry.[6] If other power reactors behave similarly to HBR, then it appears that ENDF/B-VI cross sections should replace the older library data currently in use.

The next section examines the impact of various cross-section libraries on RPV dosimeter calculations.

Table 3.1 Absolute spectra at 20° surveillance location in HBR Cycle 9
(calculated with ENDF/B-VI Fe-O-H)

Group	Upper Energy (MeV)	Group flux ($n \cdot cm^{-2} \cdot s^{-1}$)	Cumulative flux ($n \cdot cm^{-2} \cdot s^{-1}$)	Group dpa	Cumulative dpa	dpa fraction*
1	1.733E+01	6.078E+06	6.078E+06	1.776E-14	1.776E-14	3.225E-04
2	1.419E+01	2.445E+07	3.053E+07	6.469E-14	8.245E-14	1.497E-03
3	1.221E+01	9.620E+07	1.267E+08	2.317E-13	3.142E-13	5.706E-03
4	1.000E+01	1.978E+08	3.245E+08	4.389E-13	7.531E-13	1.368E-02
5	8.607E+00	3.443E+08	6.688E+08	7.185E-13	1.472E-12	2.673E-02
6	7.408E+00	8.333E+08	1.502E+09	1.619E-12	3.091E-12	5.613E-02
7	6.065E+00	1.232E+09	2.734E+09	2.198E-12	5.289E-12	9.605E-02
8	4.966E+00	2.373E+09	5.107E+09	3.728E-12	9.016E-12	1.637E-01
9	3.679E+00	1.845E+09	6.952E+09	2.528E-12	1.154E-11	2.097E-01
10	3.012E+00	1.404E+09	8.356E+09	1.784E-12	1.333E-11	2.421E-01
11	2.725E+00	1.653E+09	1.001E+10	2.108E-12	1.544E-11	2.803E-01
12	2.466E+00	8.123E+08	1.082E+10	9.520E-13	1.639E-11	2.976E-01
13	2.365E+00	2.338E+08	1.106E+10	2.562E-13	1.664E-11	3.023E-01
14	2.346E+00	1.144E+09	1.220E+10	1.191E-12	1.784E-11	3.239E-01
15	2.231E+00	3.124E+09	1.532E+10	3.230E-12	2.107E-11	3.826E-01
16	1.920E+00	3.719E+09	1.904E+10	3.025E-12	2.409E-11	4.375E-01
17	1.653E+00	5.420E+09	2.446E+10	4.392E-12	2.848E-11	5.173E-01
18	1.353E+00	9.931E+09	3.439E+10	5.565E-12	3.405E-11	6.183E-01
19	1.003E+00	6.900E+09	4.129E+10	2.529E-12	3.658E-11	6.643E-01
20	8.208E-01	3.349E+09	4.464E+10	1.879E-12	3.845E-11	6.984E-01
21	7.427E-01	9.370E+09	5.401E+10	3.386E-12	4.184E-11	7.599E-01
22	6.081E-01	7.901E+09	6.191E+10	2.325E-12	4.417E-11	8.021E-01
23	4.979E-01	8.370E+09	7.029E+10	3.318E-12	4.748E-11	8.624E-01
24	3.688E-01	7.584E+09	7.787E+10	1.568E-12	4.905E-11	8.908E-01
25	2.972E-01	1.121E+10	8.908E+10	2.248E-12	5.130E-11	9.317E-01
26	1.832E-01	9.518E+09	9.860E+10	1.342E-12	5.264E-11	9.560E-01
27	1.111E-01	7.375E+09	1.060E+11	9.536E-13	5.360E-11	9.734E-01
28	6.738E-02	6.268E+09	1.122E+11	4.060E-13	5.400E-11	9.807E-01
29	4.087E-02	2.409E+09	1.147E+11	1.949E-13	5.420E-11	9.843E-01
30	3.183E-02	1.178E+09	1.158E+11	3.349E-13	5.453E-11	9.904E-01
31	2.606E-02	2.151E+09	1.180E+11	4.337E-14	5.458E-11	9.911E-01
32	2.418E-02	1.272E+09	1.193E+11	5.571E-15	5.458E-11	9.912E-01
33	2.188E-02	3.426E+09	1.227E+11	2.806E-14	5.461E-11	9.918E-01
34	1.503E-02	6.526E+09	1.292E+11	1.224E-13	5.473E-11	9.940E-01
35	7.102E-03	7.034E+09	1.362E+11	6.257E-14	5.479E-11	9.951E-01
36	3.355E-03	6.511E+09	1.427E+11	2.292E-14	5.482E-11	9.955E-01
37	1.585E-03	1.094E+10	1.537E+11	1.840E-14	5.484E-11	9.959E-01
38	4.540E-04	5.733E+09	1.594E+11	5.652E-16	5.484E-11	9.959E-01
39	2.144E-04	6.400E+09	1.658E+11	9.177E-16	5.484E-11	9.959E-01
40	1.013E-04	8.475E+09	1.743E+11	1.891E-15	5.484E-11	9.959E-01
41	3.727E-05	1.038E+10	1.847E+11	4.088E-15	5.484E-11	9.960E-01
42	1.068E-05	5.944E+09	1.906E+11	3.821E-15	5.485E-11	9.961E-01
43	5.043E-06	7.414E+09	1.980E+11	7.414E-15	5.485E-11	9.962E-01
44	1.855E-06	4.935E+09	2.030E+11	7.585E-15	5.486E-11	9.963E-01
45	8.764E-07	4.435E+09	2.074E+11	9.952E-15	5.487E-11	9.965E-01
46	4.140E-07	4.520E+09	2.119E+11	1.771E-14	5.489E-11	9.968E-01
47	1.000E-07 **	1.857E+10	2.305E+11	1.736E-13	5.506E-11	1.000E+00

* Cumulative dpa normalized to 1.0

** Lower energy boundary for group 47 = 1.0 E-11

Table 3.2 Absolute spectra at 0° cavity location in HBR Cycle 9
(calculated with ENDF/B-VI Fe-O-H)

Group	Upper Energy (MeV)	Group flux ($n \cdot cm^{-2} \cdot s^{-1}$)	Cumulative flux ($n \cdot cm^{-2} \cdot s^{-1}$)	Group dpa	Cumulative dpa	dpa fraction*
1	1.733E+01	9.219E+04	9.219E+04	2.694E-16	2.694E-16	1.058E-04
2	1.419E+01	3.544E+05	4.466E+05	9.377E-16	1.207E-15	4.741E-04
3	1.221E+01	1.237E+06	1.684E+06	2.980E-15	4.187E-15	1.644E-03
4	1.000E+01	2.342E+06	4.026E+06	5.197E-15	9.384E-15	3.685E-03
5	8.607E+00	3.542E+06	7.567E+06	7.391E-15	1.678E-14	6.588E-03
6	7.408E+00	7.086E+06	1.465E+07	1.377E-14	3.054E-14	1.199E-02
7	6.065E+00	9.813E+06	2.447E+07	1.751E-14	4.805E-14	1.887E-02
8	4.966E+00	1.887E+07	4.333E+07	2.964E-14	7.769E-14	3.051E-02
9	3.679E+00	1.599E+07	5.933E+07	2.191E-14	9.960E-14	3.912E-02
10	3.012E+00	1.316E+07	7.249E+07	1.673E-14	1.163E-13	4.568E-02
11	2.725E+00	1.666E+07	8.915E+07	2.124E-14	1.376E-13	5.403E-02
12	2.466E+00	8.788E+06	9.793E+07	1.030E-14	1.479E-13	5.807E-02
13	2.365E+00	2.975E+06	1.009E+08	3.260E-15	1.511E-13	5.935E-02
14	2.346E+00	1.498E+07	1.159E+08	1.559E-14	1.667E-13	6.547E-02
15	2.231E+00	4.148E+07	1.574E+08	4.289E-14	2.096E-13	8.232E-02
16	1.920E+00	6.640E+07	2.238E+08	5.400E-14	2.636E-13	1.035E-01
17	1.653E+00	1.125E+08	3.363E+08	9.120E-14	3.548E-13	1.393E-01
18	1.353E+00	3.094E+08	6.457E+08	1.734E-13	5.282E-13	2.074E-01
19	1.003E+00	3.226E+08	9.683E+08	1.182E-13	6.464E-13	2.539E-01
20	8.208E-01	1.426E+08	1.111E+09	7.997E-14	7.264E-13	2.853E-01
21	7.427E-01	8.286E+08	1.940E+09	2.995E-13	1.026E-12	4.029E-01
22	6.081E-01	7.311E+08	2.671E+09	2.151E-13	1.241E-12	4.874E-01
23	4.979E-01	8.233E+08	3.494E+09	3.264E-13	1.567E-12	6.155E-01
24	3.688E-01	1.245E+09	4.738E+09	2.574E-13	1.825E-12	7.166E-01
25	2.972E-01	1.462E+09	6.200E+09	2.931E-13	2.118E-12	8.317E-01
26	1.832E-01	1.355E+09	7.555E+09	1.910E-13	2.309E-12	9.067E-01
27	1.111E-01	8.587E+08	8.414E+09	1.110E-13	2.420E-12	9.503E-01
28	6.738E-02	5.844E+08	8.998E+09	3.785E-14	2.458E-12	9.652E-01
29	4.087E-02	1.982E+08	9.197E+09	1.604E-14	2.474E-12	9.715E-01
30	3.183E-02	1.209E+08	9.317E+09	3.437E-14	2.508E-12	9.850E-01
31	2.606E-02	4.346E+08	9.752E+09	8.761E-15	2.517E-12	9.884E-01
32	2.418E-02	2.587E+08	1.001E+10	1.133E-15	2.518E-12	9.889E-01
33	2.188E-02	4.159E+08	1.043E+10	3.406E-15	2.521E-12	9.902E-01
34	1.503E-02	5.199E+08	1.095E+10	9.754E-15	2.531E-12	9.941E-01
35	7.102E-03	4.995E+08	1.145E+10	4.443E-15	2.536E-12	9.958E-01
36	3.355E-03	4.213E+08	1.187E+10	1.483E-15	2.537E-12	9.964E-01
37	1.585E-03	6.134E+08	1.248E+10	1.032E-15	2.538E-12	9.968E-01
38	4.540E-04	3.002E+08	1.278E+10	2.959E-17	2.538E-12	9.968E-01
39	2.144E-04	2.930E+08	1.307E+10	4.202E-17	2.538E-12	9.968E-01
40	1.013E-04	3.590E+08	1.343E+10	8.010E-17	2.538E-12	9.968E-01
41	3.727E-05	4.006E+08	1.383E+10	1.578E-16	2.539E-12	9.969E-01
42	1.068E-05	2.146E+08	1.405E+10	1.379E-16	2.539E-12	9.970E-01
43	5.043E-06	2.439E+08	1.429E+10	2.439E-16	2.539E-12	9.971E-01
44	1.855E-06	1.521E+08	1.444E+10	2.338E-16	2.539E-12	9.972E-01
45	8.764E-07	1.273E+08	1.457E+10	2.856E-16	2.539E-12	9.973E-01
46	4.140E-07	1.277E+08	1.470E+10	5.003E-16	2.540E-12	9.975E-01
47	1.000E-07 **	6.919E+08	1.539E+10	6.468E-15	2.546E-12	1.000E+00

* Cumulative dpa normalized to 1.0

** Lower energy boundary for group 47 = 1.0 E-11

Table 3.3 Absolute dosimeter response rates for mid-cycle 9 of HBR
(calculated with ENDF/B-VI Fe-O-H and Version VI dosimeter cross sections)

Reactions	Surveillance	Cavity
$^{54}Fe(n,p)$	2.907E-15	2.690E-17
$^{58}Ni(n,p)$	3.932E-15	4.008E-17
$^{63}Cu(n,\alpha)$	2.951E-17	2.997E-19
$^{237}Np(n,f)$	8.749E-14	3.380E-15
$^{238}U(n,f)$	1.285E-14	1.793E-16
$^{46}Ti(n,p)$	4.649E-16	4.274E-18
Flux > 1.0 MeV	3.450E+10	6.509E+08
Flux > 0.1 MeV	9.860E+10	7.555E+09

Table 3.4 Ratio of dosimeter reaction rates obtained with original
SAILOR Library to values obtained with ELXSIR

	ENDF/B-VI dosimetry file		Original dosimetry file	
Dosimeter	Downcomer*	Cavity**	Downcomer*	Cavity**
$^{54}Fe(n,p)$	1.06	1.06	1.06	1.06
$^{58}Ni(n,p)$	1.09	1.10	1.06	1.12
$^{63}Cu(n,\alpha)$	1.08	1.10	1.22	1.28
$^{237}Np(n,f)$	1.02	0.76	1.06	0.81
$^{238}U(n,f)$	1.06	0.99	1.05	0.99
$^{46}Ti(n,p)$	1.04	1.06	1.11	1.12

*Surveillance Capsule at 20°.
**0° cavity location, R = 238.02 cm.

Table 3.5 Ratio of dosimeter reaction rates obtained with SAILOR (ENDF/B-VI Fe-O-H) to values obtained with ELXSIR

	ENDF/B-VI dosimetry file		Original dosimetry file	
Dosimeter	Downcomer*	Cavity**	Downcomer*	Cavity**
$^{54}Fe(n,p)$	1.19	1.43	1.18	1.42
$^{58}Ni(n,p)$	1.21	1.47	1.18	1.50
$^{63}Cu(n,\alpha)$	1.15	1.34	1.29	1.54
$^{237}Np(n,f)$	1.11	1.00	1.15	1.07
$^{238}U(n,f)$	1.16	1.31	1.16	1.31
$^{46}Ti(n,p)$	1.14	1.37	1.22	1.46

*Surveillance Capsule at 20°.
**0° cavity location, R = 238.02 cm.

Table 3.6 Impact of ENDF/B-VI Fe-O-H data on calculated cavity reaction rates for HBR

	SAILOR (ENDF-6 Fe-O-H)
Dosimeter	Original SAILOR
$^{54}Fe(n,p)$	1.35
$^{58}Ni(n,p)$	1.34
$^{63}Cu(n,\alpha)$	1.22
$^{237}Np(n,f)$	1.32
$^{238}U(n,f)$	1.32
$^{46}Ti(n,p)$	1.30

Table 3.7 C/E values for HBR Cycle 9

Dosimeter	Downcomer			Cavity		
	ELXSIR (Maerker)	Original* SAILOR	SAILOR ENDF/B-VI* Fe-O-H	ELXSIR (Maerker)	Original* SAILOR	SAILOR ENDF/B-VI* Fe-O-H
$^{54}Fe(n,p)$	0.83	0.88	0.98	0.68	0.72	0.97
$^{58}Ni(n,p)$	0.87	0.94	1.05	0.66	0.72	0.97
$^{63}Cu(n,\alpha)$	0.83	0.90	0.95	0.72	0.79	0.96
$^{237}Np(n,f)$	0.85	0.87	0.94	0.61	0.46	0.61
$^{238}U(n,f)$	0.80	0.85	0.93	0.65	0.65	0.86
^{46}Ti (n,p)	0.81	0.84	0.92	0.66	0.69	0.90

*SAILOR results used ENDF/B-VI dosimetry file.

4 COMPARISON OF SAILOR, ELXSIR, AND VITAMIN-E CALCULATIONS FOR A 1-D MODEL OF HBR

As indicated in the previous section, the availability of the new ENDF/B-VI iron cross-section data will have a major impact on transport calculations of RPV fluence. Initial results from this study indicate that the differences in the basic ENDF/B data in version VI compared with either version IV or V will improve agreement with the measured HBR dosimetry. The earlier two versions of ENDF/B (IV and V) form the basis of several cross-section libraries that have been used for years to analyze the fluence accumulated by power reactors. Some of the commonly used libraries for RPV transport calculations are SAILOR, ELXSIR, and VITAMIN-E.[10]

The first two were collapsed from the ENDF/B-IV based VITAMIN-C library, while VITAMIN-E, a fine-group library, is based on ENDF/B-V. As pointed out in Section 3, in the course of this study it was observed that unexpected differences occur even among some of the results obtained with the ELXSIR and the SAILOR cross-section libraries, even though the basic ENDF/B data from which these are processed are similar. These observations suggest that factors other than merely the differences between ENDF/B-VI and the earlier ENDF/B version may affect the multigroup cross-section data used by various organizations performing RPV fluence analysis.

As part of the continuing effort to understand the causes for discrepancies between different transport calculations of RPV dosimetry, a set of 1-D calculations was performed for H.B. Robinson using SAILOR (47 groups), ELXSIR (56 groups), and VITAMIN-E (174 groups). None of the calculations use ENDF/B-VI data (i.e., SAILOR and ELXSIR are based on version IV and VITAMIN-E on version V). Hence, all three libraries are based on similar evaluated data for the energy range of interest. The purpose of this analysis is to:

1. examine sensitivity of RPV transport calculations to iron cross-section self-shielding and weighting spectra;

2. compare both SAILOR and ELXSIR calculations with VITAMIN-E to see which agrees better with a fine group calculation;

3. quantify the differences caused by the original SAILOR and ELXSIR libraries on the flux spectrum in the cavity; and

4. explain why the SAILOR results in this study differ from Maerker's earlier ELXSIR calculations.

All transport calculations use the identical model, normalization and source spectrum (a ^{235}U Watt spectrum based on ENDF/B-V) to ensure that the observed differences reflect only the effect of the cross-section library differences.

First consider the impact of self-shielding on the VITAMIN-E calculations, as shown in Table 4.1. The first column of results used no self-shielding of the library in computing the cavity flux; the second column is the ratio indicating how much the computed values of flux above 1 MeV and above 0.1 MeV, respectively, will increase if the cross sections are self-shielded correctly. The third column shows how much the integral flux values differ if the RPV iron data were self-shielded like stainless steel (SS) rather than carbon steel (CS). It can be seen that self-shielding the cross sections has a large impact on the computed cavity fluxes, even in the high-energy range above 1 MeV — the value of ϕ (>1) increases 25% and ϕ (>0.1) increases 37%. Presumably it is the impact of the self-shielding on the resonances present in the iron inelastic cross section between 800 eV and 2 MeV that is causing the greatest effect on the integral fluxes. At energies slightly above 2 MeV, no resolved resonance structure is shown in the iron inelastic data in ENDF/B-V. The integral fluxes are not so sensitive to resonances in the iron elastic data. The effect of self-shielding the RPV data for a SS mixture rather than the actual CS mixture is only worth about 5% in the cavity for ϕ (>1) and about 10% for ϕ (>0.1).

In the ELXSIR library, two types of weighted iron cross sections are included. The one labeled "*REM Shielded Problem*" is recommended for use in CS and the one called "*Combined CTR and CRBR Processing*" is for SS. Table 4.2 shows the effect of using the two differently weighted cross sections for the RPV iron data in the

transport calculations. The SS-weighted iron produces cavity ϕ (>1) and ϕ (>0.1) that are 4% and 8% lower, respectively, than obtained with the CS-weighted data. These differences are close to those noted as a result of differences in self-shielding for SS vs CS in VITAMIN-E. This observation suggests that most of the differences between the CS-and SS-weighted-group cross sections are probably caused by differences in self-shielding rather than differences in the spectrum used to collapse the fine-group data. If the incorrectly weighted iron data were used in the ELXSIR calculations, a small discrepancy is introduced in the computed cavity flux.

Next, examine the impact of using SAILOR vs ELXSIR cross sections in computing the cavity flux and dosimeter activities. These conclusions are significant because SAILOR is widely used in industry for RPV fluence calculations, while ELXSIR has been used in several benchmark and sensitivity studies produced by ORNL (Maerker); hence it is important to know how to correlate the results obtained by various organizations.

Table 4.3 shows results obtained for several integral fluxes in the cavity, using the standard SAILOR and ELXSIR libraries (both of which were derived from ENDF/B-IV) and the VITAMIN-E fine group results. The VITAMIN-E values are considered to be the most accurate because of the large number of multigroups.

It can be seen that the integrated flux above 2.35 MeV is calculated only slightly lower with ELXSIR than SAILOR; therefore, the threshold dosimeters ^{54}Fe(n,p), ^{58}Ni(n,p) and ^{63}Cu(n,α) will be perhaps a little lower in the ELXSIR. Overall, however, the SAILOR, ELXSIR, and VITAMIN-E all agree well in the energy range above 2 MeV. Note however, that the integrated flux above 1 MeV is about 8% higher in the ELXSIR calculation compared with SAILOR, and the ELXSIR value agrees well with VITAMIN-E. The SAILOR value for ϕ (>1.0) appears to be underestimated by about 9% compared with VITAMIN-E. Surprisingly, the flux above 0.1 MeV is calculated about 20% higher with ELXSIR compared with SAILOR! When compared with VITAMIN-E, SAILOR underestimates the value for ϕ (>0.1) by about 16%. The fact that SAILOR underestimates the flux between 0.1 and 2.0 MeV when compared with ELXSIR and VITAMIN-E will cause the lower threshold dosimeters, such as ^{238}U(n,f), and especially ^{237}Np(n,f), to be calculated low. Table 4.4 compares the calculated values for the neptunium fission rate. It can be seen that the ELXSIR calculation is about 20% higher than SAILOR and agrees within 6% of the VITAMIN-E value. The SAILOR value is about 12% lower than VITAMIN-E. [Note: all three calculations used the same ^{237}Np(n,f) cross sections.] The discrepancies between SAILOR and ELXSIR below 2 MeV are probably caused by the different group structures in the two libraries, because the impact of the different collapsing and self-shielding procedure is small. Table 4.5 shows the group structures of VITAMIN-E. Table 4.6 shows the group structures of ELXSIR and SAILOR. The ELXSIR library contains two more energy groups than SAILOR in the energy range between 0.11 and 1.0 MeV and the bounderies are arranged somewhat differently.

Recall that the results given in Section 3 for the ^{237}Np(n,f) dosimeters in the HBR cavity, which were performed with the original SAILOR library, do not seem to be consistent with Maerker's earlier calculations done with ELXSIR. For example, our ^{237}Np value in the cavity is about 24% lower than the value computed by Maerker. It now appears that the discrepancy is caused by differences in the group structure of the two libraries. Table 4.4 indicates the ELXSIR library produces a neptunium reaction rate about 20% higher than the corresponding SAILOR value, due to a higher flux between 0.1 and 2 MeV. These results suggest that the 47-neutron group structure in SAILOR may not be fine enough in the energy range 0.1 to 2.0 MeV. This is evidenced by the fact that the SAILOR fluxes do not agree with the VITAMIN-E values in this energy range, while the ELXSIR does agree with the fine-group calculation. The fine-group VITAMIN-E results could be used to obtain a correction factor for the error introduced by the coarse-group structure in SAILOR. Based on the VITAMIN-E to SAILOR ratio in Table 4.4, the SAILOR ^{237}Np values cited in Table 3.7 for the cavity dosimeter should be increased by about 14% (i.e., 1/0.88). This correction assumes that the ENDF/B-VI SAILOR values will scale by the same factor as the original SAILOR results, and that the 2-D calculations can be scaled by a 1-D calculation. Therefore, our best estimate for the C/E ratios of the ^{237}Np cavity dosimeters are 0.69 for the ENDF/B-VI SAILOR results and 0.52 for the original SAILOR results. It can be seen that our best estimate for the calculated ^{237}Np activity in the cavity position is substantially lower than the reported measured value. Because the calculated values obtained with the ENDF/B-VI Fe-O-H SAILOR library agree well with the measured results for the other dosimeters, an experimental discrepancy is suspected for the neptunium activity.

Table 4.1 Impact of self-shielding on fine-group VITAMIN-E calculations in 1-D HBR model

	No shielding ($n \cdot cm^{-2} \cdot s^{-1}$)	Shielding: None ($n \cdot cm^{-2} \cdot s^{-1}$)	SS-shielded RPV / CS-shielded RPV
Cavity ϕ(E>1.0MeV)	2.45E-4	1.25	0.95
Cavity ϕ(E>0.1MeV)	4.09E-3	1.37	0.90

Table 4.2 Impact of different cross-section weighting on ELXSIR calculations in 1-D HBR model

	CS-weighted RPV iron ($n \cdot cm^{-2} \cdot s^{-1}$)	SS-weighted RPV iron ($n \cdot cm^{-2} \cdot s^{-1}$)	Ratio (SS/CS)
Cavity ϕ(E>1.0 MeV)	3.01E-4	2.89E-4	0.96
Cavity ϕ(E>0.1 MeV)	5.67E-3	5.28E-3	0.93

Table 4.3 Comparison of SAILOR and ELXSIR calculations for cavity integral fluxes in 1-D HBR model

Cumulative flux energy threshold (MeV)	ELXSIR / SAILOR	SAILOR / VITAMIN-E	ELXSIR / VITAMIN-E
5.00	0.97	1.01	0.98
3.00	0.97	1.04	1.00
2.35	0.99	1.00	1.00
1.90	1.01	0.95	0.96
1.65	1.03	0.95	0.98
1.35	1.06	0.92	0.98
1.00	1.08	0.91	0.98
0.80	1.11	0.91	1.01
0.50	1.20	0.89	1.07
0.10	1.20	0.84	1.01

Table 4.4 Comparison of SAILOR and ELXSIR calculations for cavity ^{237}Np(n,f) in 1-D HBR model

ELXSIR / SAILOR	SAILOR / VITAMIN-E	ELXSIR / VITAMIN-E
1.20	0.88	1.06

Table 4.5 VITAMIN-E group structures

VITAMIN-E							
GP	Upper E (eV)	GP	Upper E (eV)	GP	Upper E (eV)	GP	Upper E (eV)
1	1.9640E+07	51	1.8268E+06	101	1.2907E+05	151	1.0130E+02
2	1.7332E+07	52	1.7377E+06	102	1.2277E+05	152	7.8893E+01
3	1.6905E+07	53	1.6530E+06	103	1.1679E+05	153	6.1442E+01
4	1.6487E+07	54	1.5724E+06	104	1.1109E+05	154	4.7851E+01
5	1.5683E+07	55	1.4957E+06	105	9.8037E+04	155	3.7266E+01
6	1.4918E+07	56	1.4227E+06	106	8.6517E+04	156	2.9023E+01
7	1.4550E+07	57	1.3534E+06	107	8.2503E+04	157	2.2603E+01
8	1.4191E+07	58	1.2874E+06	108	7.9499E+04	158	1.7604E+01
9	1.3840E+07	59	1.2246E+06	109	7.1998E+04	159	1.3710E+01
10	1.3499E+07	60	1.1648E+06	110	6.7379E+04	160	1.0677E+01
11	1.2523E+07	61	1.1080E+06	111	5.6562E+04	161	8.3153E+00
12	1.2214E+07	62	1.0026E+06	112	5.2475E+04	162	6.4760E+00
13	1.1618E+07	63	9.6164E+05	113	4.6309E+04	163	5.0435E+00
14	1.1052E+07	64	9.0718E+05	114	4.0868E+04	164	3.9279E+00
15	1.0513E+07	65	8.6294E+05	115	3.4307E+04	165	3.0590E+00
16	1.0000E+07	66	8.2085E+05	116	3.1828E+04	166	2.3824E+00
17	9.5123E+06	67	7.8082E+05	117	2.8501E+04	167	1.8554E+00
18	9.0484E+06	68	7.4274E+05	118	2.7000E+04	168	1.4450E+00
19	8.6071E+06	69	7.0651E+05	119	2.6058E+04	169	1.1253E+00
20	8.1873E+06	70	6.7206E+05	120	2.4788E+04	170	8.7643E–01
21	7.7880E+06	71	6.3928E+05	121	2.4176E+04	171	6.8256E–01
22	7.4082E+06	72	6.0810E+05	122	2.3579E+04	172	5.3158E–01
23	7.0469E+06	73	5.7844E+05	123	2.1875E+04	173	4.1399E–01
24	6.7032E+06	74	5.5023E+05	124	1.9305E+04	174	1.0000E–01
25	6.5924E+06	75	5.2340E+05	125	1.5034E+04		
26	6.3763E+06	76	4.9787E+05	126	1.1709E+04		
27	6.0653E+06	77	4.5049E+05	127	1.0333E+04		
28	5.7695E+06	78	4.0762E+05	128	9.1188E+03		
29	5.4881E+06	79	3.8774E+05	129	7.1017E+03		
30	5.2205E+06	80	3.6883E+05	130	5.5308E+03		
31	4.9659E+06	81	3.3373E+05	131	4.3074E+03		
32	4.7237E+06	82	3.0197E+05	132	3.7074E+03		
33	4.4933E+06	83	2.9849E+05	133	3.3546E+03		
34	4.0657E+06	84	2.9721E+05	134	3.0354E+03		
35	3.6788E+06	85	2.9452E+05	135	2.7465E+03		
36	3.3287E+06	86	2.8725E+05	136	2.6126E+03		
37	3.1664E+06	87	2.7324E+05	137	2.4852E+03		
38	3.0119E+06	88	2.4724E+05	138	2.2487E+03		
39	2.8651E+06	89	2.3518E+05	139	2.0347E+03		
40	2.7253E+06	90	2.2371E+05	140	1.5846E+03		
41	2.5924E+06	91	2.1280E+05	141	1.2341E+03		
42	2.4660E+06	92	2.0242E+05	142	9.6112E+02		
43	2.3852E+06	93	1.9255E+05	143	7.4852E+02		
44	2.3653E+06	94	1.8316E+05	144	5.8295E+02		
45	2.3457E+06	95	1.7422E+05	145	4.5400E+02		
46	2.3069E+06	96	1.6573E+05	146	3.5357E+02		
47	2.2313E+06	97	1.5764E+05	147	2.7536E+02		
48	2.1225E+06	98	1.4996E+05	148	2.1445E+02		
49	2.0190E+06	99	1.4264E+05	149	1.6702E+02		
50	1.9205E+06	100	1.3569E+05	150	1.3007E+02		

Table 4.6 ELXSIR and SAILOR group structures

ELXSIR				SAILOR	
GP	Upper E (eV)	GP	Upper E (eV)	GP	Upper E (eV)
1	1.7333E+07	48	1.1709E+04	1	1.733+07
2	1.4191E+07	49	7.1017E+03	2	1.419+07
3	1.2214E+07	50	5.5308E+03	3	1.221+07
4	1.1052E+07	51	3.3546E+03	4	1.000+07
5	1.0000E+07	52	2.6123E+03	5	8.607+06
6	8.6071E+06	53	1.5846E+03	6	7.408+06
7	8.1873E+06	54	1.1013E+02	7	6.065+06
8	7.4082E+06	55	1.0677E+01	8	4.966+06
9	7.0469E+06	56	4.1399E-01	9	3.679+06
10	6.0653E+06			10	3.012+06
11	4.9659E+06			11	2.725+06
12	4.0657E+06			12	2.466+06
13	3.6788E+06			13	2.365+06
14	3.0119E+06			14	2.346+06
15	2.7253E+06			15	2.231+06
16	2.5924E+06			16	1.920+06
17	2.4660E+06			17	1.653+06
18	2.3653E+06			18	1.353+06
19	2.3457E+06			19	1.003+06
20	2.2313E+06			20	8.208+05
21	2.1224E+06			21	7.427+05
22	1.9205E+06			22	6.081+05
23	1.8268E+06			23	4.979+05
24	1.6530E+06			24	3.688+05
25	1.4957E+06			25	2.972+05
26	1.3534E+06			26	1.832+05
27	1.2246E+06			27	1.111+05
28	1.0026E+06			28	6.738+04
29	9.0718E+05			29	4.087+04
30	8.2085E+05			30	3.183+04
31	7.4274E+05			31	2.606+04
32	6.0810E+05			32	2.418+04
33	4.9787E+05			33	2.188+04
34	3.6883E+05			34	1.503+04
35	3.0197E+05			35	7.102+03
36	2.1280E+05			36	3.355+03
37	1.8316E+05			37	1.585+03
38	1.1109E+05			38	4.540+02
39	9.8037E+04			39	2.144+02
40	8.6517E+04			40	1.013+02
41	6.7379E+04			41	3.727+01
42	4.0068E+04			42	1.068+05
43	3.4307E+04			43	5.043+00
44	2.6058E+04			44	1.855+00
45	2.4176E+04			45	8.764+01
46	2.1875E+04			46	4.140+01
47	1.5034E+04			47	1.000+01

5 SUMMARY AND CONCLUSIONS

The calculations performed with selected ENDF/B-VI data in this study have resolved most of the discrepancies between the measured and computed dosimeter activities that were reported earlier for Cycle 9 of H. B. Robinson. The earlier analysis used the 56-group ELXSIR library, which is based on ENDF/B-IV data, and obtained calculated results that were substantially lower than the measured activities in the cavity. The 47-group ENDF/B-VI calculations in this study give values that are about 25% higher than the corresponding dosimeter activities obtained in the earlier work. The C/E values from the ENDF/B-VI calculations agree within 10% of the measured dosimeter activities at both the downcomer and cavity measurement locations, except for the ^{237}Np(n,f) cavity dosimeter which is 39% too low. It was also discovered that the ^{237}Np results calculated with the original 47-group SAILOR cross section differ from those obtained with ELXSIR, which is also based on ENDF/B-IV. This appears to be mostly a result of the difference in the group structure of the two libraries. The ELXSIR values agree better with fine-group calculations. It appears that the Np cavity dosimeter activity computed with the SAILOR library should be increased by about 14% in order to correct for its relatively coarse-group structure between 0.5 and 2.0 MeV. If this correction is applied to the ENDF/B-VI calculation, then the C/E value for the neptunium becomes 0.69, which is still about 31% low. The remaining discrepancy is believed to be caused by a problem with the experimental measurement.

It is concluded that the ENDF/B-VI cross-section data substantially improve the accuracy of the neutron transport calculations for H. B. Robinson Cycle 9. For this particular reactor, as is the case in several other reactors studied earlier, the original SAILOR and ELXSIR data give an underestimate for the cavity dosimeter values, while ENDF/B-VI gives very good agreement with the experimental results. Another important conclusion of this study is that the SAILOR group structure appears to be too coarse below 2 MeV, and this can cause discrepancies in low threshold responses computed with SAILOR compared to ELXSIR.

Although several additional reactors should be analyzed prior to making a definitive assessment of using ENDF/B-VI versus earlier evaluations, the preliminary indications suggest that RPV fluence predictions may be enhanced by establishing a "standard library" based on ENDF/B-VI data for use by all organizations involved with pressure vessel lifetime determination. Some thought must also be given to the appropriate group structure and processing methodology for a new library in light of the apparent inconsistency with the SAILOR and ELXSIR libraries.

REFERENCES

1. R. E. Maerker, *LEPRICON Analysis of Pressure Vessel Surveillance Dosimetry Inserted into H. B. Robinson-2 during Cycle 9*, NUREG/CR-4439, ORNL/TM-10132, U.S. Nuclear Regulatory Commission, August 1986.

2. M. L. Williams, R. L. Childs, and M. Asgari, *Analysis of H. B Robinson PWR Vessel Fluence for Cycle 10 Utilizing Partial Length Shield Assemblies*, NUREG/CR-5530, U.S. Nuclear Regulatory Commission, 1990.

3. M. L. Williams et al., *The ELXSIR Cross-Section Library for LWR Pressure Vessel Irradiation Studies: Part of the LEPRICON Computer Code System*, EPRI NP-3654, Electric Power Research Institute, 1984.

4. G. L. Simmons and R. W. Roussin, *RSIC Data Library Collection – SAILOR–Coupled, Self-Shielded, 47 Neutron, 20 Gamma-Ray, P_3 Cross-Section Library for Light Water Reactors*, DLC-76, Radiation Shielding Information Center, Oak Ridge National Laboratory, 1985.

5. C. Y. Fu and D. M. Hetrick, *Update of ENDF/B-V Mod-3 Iron: Neutron-Producing Reaction Cross Sections and Energy-Angle Correlations*, ORNL/TM-9964 (ENDF-341), Martin Marietta Energy Systems, Inc., Oak Ridge Natl. Lab., 1986.

6. M. L. Williams et al., "Transport Calculations of Neutron Transmission Through Steel Using ENDF/B-V, Revised ENDF/B-V, and ENDF/B-VI Iron Evaluations," *Annals Nucl. En.*, Vol. 18, pp. 549-565, 1991.

7. R. W. Roussin et al., *VITAMIN-C: The CTR Processed Multigroup Cross-Section Library for Neutronics Studies*, ORNL/RSIC-37, Union Carbide Corp., Nucl. Div., Oak Ridge Natl. Lab., 1980.

8. F. W. Stallmann, *LSL-M2 Least-Squares Logarithmic Adjustment of Neutron Spectra*, Radiation Shielding Information Center, Oak Ridge National Laboratory, PSR-233 Micro, 1985.

9. E. P. Lippincott et al., *Evaluation of Surveillance Capsule and Reactor Cavity Dosimetry from H. B. Robinson Unit 2, Cycle 9, NUREG/CR-4576, WCAP-11104, Westinghouse Corp., February 1987.*

10. C. R. Weisbin et al., *VITAMIN-E: An ENDF/B-V Multigroup Cross-Section Library for LMFBR Core and Shield, LWR Shield, Dosimetry and Fusion Blanket Technology*, ORNL-5505 (ENDF-274), Union Carbide Corp., Nucl. Div., Oak Ridge Natl. Lab., 1979.

NUREG/CR-6071
Version 1
ORNL/TM-12406
Dist. Category R5

INTERNAL DISTRIBUTION

1.	B. R. Appleton
2.	W. R. Corwin
3.	S. K. Iskander
4-23.	F. B. K. Kam
24.	R. K. Nanstad
25.	W. E. Pennell
26.	C. E. Pugh
27.	I. Remec
28.	C. H. Shappert
29-32.	F. W. Stallmann
33-36.	J. A. Wang
37.	R. M. Westfall
38.	G. E. Whitesides
39.	Central Research Library
40.	ORNL Y-12 Research Library Document Reference Section
41-42.	Laboratory Records Departyment
43.	Laboratory Records, ORNL (RC)
44.	ORNL Patent Office

EXTERNAL DISTRIBUTION

45. Ait Abderrahim, SCK/CEN Fuel Research Unit, Boeretang, 200B-2400 MOL, Belgium

46. S. L. Anderson, Radiation and Environmental Systems, Westinghouse Electric Corporation, Nuclear Energy Systems, Monroeville Nuclear Center, P.O. Box 355, Pittsburgh, PA 15230

47. M. Asgari, Louisiana State University, Nuclear Science Center, Baton Rouge, LA 70803

48. J. F. Carew, Bldg. 130 Department of Nuclear Engineering, Brookhaven National Laboratory, Upton Long Island, New York 11973

49. G. P. Cavanaugh, Combustion Engineering, Inc., Dept. 9492-425, 1000 Prospect Hill Rd., Windsor, CT 06095

50. J. Helm, Dept. of Applied Physics & Nuclear Engineering, 202 Mudd, Columbia University, New York, New York 10027

51. A. Hiser, U.S. Nuclear Regulatory Commission, Division of Engineering, Mail Stop NL S 217 C, Washington, DC 20555

52. W. C. Hopkins, Bechtel Corporation, 9801 Washingtonian Blvd., Gaithersburg, MD 20878-5356

53. K. D. Ilieva, Academy of Science, Institute of Nuclear Research and Nuclear Energy, Boul, Tzarigradsko, Shausce 72

54. E. P. Lippincott, Westinghouse Electric Corporation, M/S E4-33, Westinghouse Energy Center, P.O. Box 355, Pittsburgh, PA 15230-0355

55. L. Lois, U.S. Nuclear Regulatory Commission, Phillips Building, MS P-924, Washington, DC 20555

56. M. Mayfield, U.S. Nuclear Regulatory Commission, Division of Engineering, Mail Stop NL S 217 C, Washington, DC 20555

57. E. D. McGarry, National Institute of Standards and Technology, Bldg. 235-A155, Gaithersburg, MD 20899

58. B. Osmera, Nuclear Research Institute, Narcony Trida 3, 250 68 Rez, Czechoslovakia

59. J. Rataj, 250 68 Rez, Czechoslovakia

60. E. Sajo, Louisiana State University, Nuclear Science Center, Baton Rouge, LA 70803

61. C. Z. Serpan, Jr., U.S. Nuclear Regulatory Commission, Division of Engineering, Mail Stop NL S 217C, Washington, DC 20555

62. Al Taboada, U.S. Nuclear Regulatory Commission, Division of Engineering, Mail Stop NL S 217 C, Washington, DC 20555

63. M. L. Williams, Louisiana State University, Nuclear Science Center, Baton Rouge, LA 70803

64. S. Zaritsky, Kurchatov Institute, Kurchatov Square, 123182 Moscow, Russia

65. E. Zsolnay, Technical University of Budapest, BME H-1521 Budapest, Muegytem RKP9, Hungary

66. Office of the Deputy Assistant Manger for Energy, Research and Development, Department of Energy Oak Ridge Operations (DOE-ORO), P.O. Box 2008, Oak Ridge, TN 37831-6269

67-68. Office of Scientific and Technical Information, P.O. Box 62, Oak Ridge, TN 37831

NRC FORM 335 (2-89) NRCM 1102, 3201, 3202

U.S. NUCLEAR REGULATORY COMMISSION

BIBLIOGRAPHIC DATA SHEET

(See instructions on the reverse)

1. REPORT NUMBER (Assigned by NRC, Add Vol., Supp., Rev., and Addendum Numbers, if any.)
NUREG/CR-6071
ORNL/TM-12406

2. TITLE AND SUBTITLE
Impact of ENDF/B-VI Cross-Section Data on H. B. Robinson Cycle 9 Dosimetry Calculations

3. DATE REPORT PUBLISHED
MONTH: October
YEAR: 1993

4. FIN OR GRANT NUMBER
B0415

5. AUTHOR(S)
M. L. Williams*, M. Asgari*, F. B. Kam

6. TYPE OF REPORT
Technical

7. PERIOD COVERED *(Inclusive Dates)*

8. PERFORMING ORGANIZATION – NAME AND ADDRESS *(If NRC, provide Division, Office or Region, U.S. Nuclear Regulatory Commission, and mailing address; if contractor, provide name and mailing address.)*
Oak Ridge National Laboratory
Oak Ridge, TN 37831-6285

*Louisiana State University Nuclear Science Center
Baton Rouge, LA 70803

9. SPONSORING ORGANIZATION – NAME AND ADDRESS *(If NRC, type "Same as above"; if contractor, provide NRC Division, Office or Region, U.S. Nuclear Regulatory Commission, and mailing address.)*
Division of Engineering
Office of Nuclear Regulatory Research
U.S. Nuclear Regulatory Commission
Washington, DC 20555-0001

10. SUPPLEMENTARY NOTES

11. ABSTRACT *(200 words or less)*

Dosimeters that were removed from the H. B. Robinson reactor following Cycle 9 were analyzed and compared with calculated results in an earlier study. This work updates the calculation using recently available ENDF/B-VI data in order to assess advantages to using the newer cross sections in reactor pressure vessel fluence calculations. A comparison is also made to determine the impact of various cross-section libraries on computed dosimeter activities.

Significant improvements are obtained with the ENDF/B-VI cross sections. Other factors, such as differences in group structures of multigroup libraries, may also affect the calculated dosimeter activities.

12. KEY WORDS/DESCRIPTORS *(List words or phrases that will assist researchers in locating the report.)*
H. B. Robinson, ENDF/B-VI, reactor pressure vessel, dosimeter

13. AVAILABILITY STATEMENT
Unlimited

14. SECURITY CLASSIFICATION
(This Page)
Unclassified
(This Report)
Unclassified

15. NUMBER OF PAGES

16. PRICE

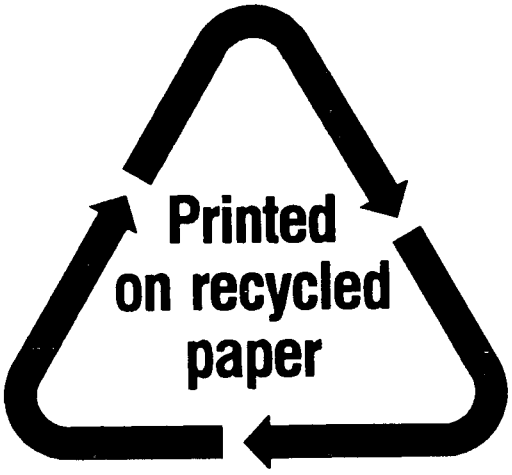

Federal Recycling Program